

CFD prediction of fire-induced hot gases in buildings

G.Q. Xiao^{1,2}, J.Y. Tu¹, G.H. Yeoh³

Abstract

A CFD model was developed to predict the fire-induced hot gas within internal narrow passages in enclosures in buildings, such as elevator shafts in buildings. Simulations were performed to predict the spatial variation of temperature and velocity distributions in this configuration. The computational results were compared against the experiments of Mercier and Jaluria (1999). Good agreement was achieved between the experimental data and model predictions. The results obtained indicated that the primary transport mechanism affecting the temperature and velocity distributions within the internal passage was due to the buoyancy effect caused by temperature difference of the airflow. In the results, a thin boundary layer was formed along the vertical wall as the Grashof number was increased while the Reynolds number was kept fixed, and the recirculation of the airflow became more pronounced in the flow field.

¹ School of Aerospace, Mechanical and Manufacturing Engineering, RMIT University, Victoria 3083, Australia

² School of Energy and Safety Engineering, Hunan University of Science and Technology, Xiangtan, Hunan, 411201, China

³ Australian Nuclear Science and Technology Organization (ANSTO), PMB 1, Menai, NSW 2234, Australia

1. INTRODUCTION

The building fire can cause considerable damage to building structures and human lives[1,2]; the principal hazard in fire is usually the spread of sooty smoke and hot toxic gas which can flow through vents, openings and internal passages such as ventilation ducts, stairwells, and elevator shafts, Although a large amount of results has been reported concerning fires in enclosures such as offices and rooms, little attention has been given to investigate fire-induced gas flows in modern high-rise buildings. Concerning the possibilities of these many flow-paths, the spilling of hot smoke and toxic gases in an open shaft of a multistorey building is investigated herein because of the imposing hazardous condition.

One possible way of studying this problem could involve a full-scale instrumentation of a building structure [3]. Nevertheless, such an approach may not deem to be feasible because of the high costs associated with construction and the demanding resources of instrumentation. With the advancements of computer resources and speeds, and rapid developments of numerical methodologies, numerical models are becoming increasingly powerful to study such problem. Despite the efforts of Kim and Jaluria [4] where they have developed a numerical model to solve the laminar flow in a large aspect ratio shaft, there have not been many comparisons with measurements. The lack of attention may be attributed to the complexity of the flow being vigorously turbulent that will significantly affect the fluid flow and heat transfer characteristics in a full-scale structure. As a result, no comparison exists between measurements and numerical models for turbulent flows.

In this paper, the application a computational fluid dynamics (CFD) model is evaluated for the fire-induced flow in a vertical shaft in buildings. Figure 1 describes the schematic configuration of the vertical model shaft. The width and height of the shaft are

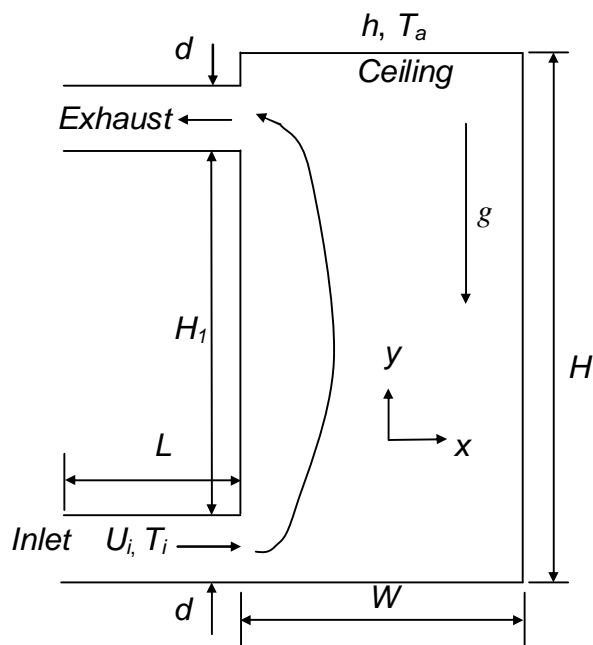


Figure 1 Schematic drawing of the vertical shaft configuration

0.5 m and 1.5 m while the height and length of inlet and outlet are 0.05 m and 0.3 m respectively. The distance between the outlet and the ceiling of the shaft is 0.1 m. The calculated air flow velocities and temperatures of the model in laminar conditions are simulated and verified against the experiment data obtained by Mercier and Jaluria [5]. A parametric investigation is performed on the velocity and temperature fields by varying the Grashof (Gr) number or Reynolds (Re) number. For the case of turbulent flow, the standard two-equation k - ϵ turbulent model [6] is employed and the predicted flow fields are compared against those in laminar conditions.

2. COMPUTATIONAL MODELS

A generic CFD commercial code, FLUENT [7], is utilised to predict the continuum gas phase of the velocity and temperature profiles under unsteady and incompressible conditions through solutions to the conservation of mass, momentum and energy. The buoyancy force due to gravity is accounted by invoking the Boussinesq approximation in the momentum equation. A two-dimensional model is adopted for the current simulation. The governing equations under consideration can be written in non-dimensional form as:

$$\frac{\partial U}{\partial X} + \frac{\partial V}{\partial Y} = 0 \quad (1)$$

$$\frac{\partial U}{\partial t_c} + \frac{\partial(UU)}{\partial X} + \frac{\partial(UV)}{\partial Y} = -\frac{\partial P}{\partial X} + \left\{ \frac{1}{Re} + \frac{1}{Re_t} \right\} \left(\frac{\partial^2 U}{\partial X^2} + \frac{\partial^2 U}{\partial Y^2} \right) \quad (2)$$

$$\frac{\partial V}{\partial t_c} + \frac{\partial(UV)}{\partial X} + \frac{\partial(VV)}{\partial Y} = -\frac{\partial P}{\partial Y} + \left\{ \frac{1}{Re} + \frac{1}{Re_t} \right\} \left(\frac{\partial^2 V}{\partial X^2} + \frac{\partial^2 V}{\partial Y^2} \right) + \frac{Gr}{Re^2} \Theta \quad (3)$$

$$\frac{\partial \Theta}{\partial t_c} + \frac{\partial(U\Theta)}{\partial X} + \frac{\partial(V\Theta)}{\partial Y} = \left\{ \frac{1}{Pe} + \frac{1}{Pe_t} \right\} \left(\frac{\partial^2 \Theta}{\partial X^2} + \frac{\partial^2 \Theta}{\partial Y^2} \right) \quad (4)$$

The following non-dimensional variables are given by:

$$X = \frac{x}{H}; \quad Y = \frac{y}{H}; \quad U = \frac{u}{U_i}; \quad V = \frac{v}{U_i}; \quad P = \frac{P}{\rho U_i^2}; \quad \tau_c = \frac{t}{H/U_i}; \quad \Theta = \frac{T - T_a}{\Delta T}$$

where the lower-case letters denote the dimensional variables. The velocity components u and v correspond to the x and y directions of the Cartesian coordinate system while the dimensionless time t_c is defined as the convective timescale. The non-dimensional parameters in the above equations are defined as: the laminar and turbulent Reynolds numbers – $Re = U_i H / \nu$ and $Re_t = U_i H / \nu_t$; the Grashof number – $g b \Delta T H^3 / \nu^2$; and the laminar and turbulent Péclet numbers – $Pe = Re Pr$ and $Pe_t = Re_t Pr_t$. The kinematic viscosity of the fluid is denoted by ν , the coefficient of volumetric expansion by b and the temperature difference between the temperatures at the inlet and ambient condition by $\Delta T = (T_i - T_a)$.

For laminar flow, the turbulent Reynolds and Péclet numbers diminish in the momentum and energy equations. Nevertheless, for turbulent flow, the eddy-viscosity concept is employed for the representation of the turbulent Reynolds and Péclet numbers in the governing equations due to turbulence. This is expressed by the solution of the standard k - ϵ turbulent model with additional source terms to account for buoyancy effects. At the inlet, a uniform unidirectional velocity U_i and temperature T_i are prescribed, the outlet conditions that involve setting the continuity equation and relative pressure to be zero at the top exhaust boundary[8] (see Figure 1). Neumann condition is imposed for the case of outflow while Dirichlet condition is applied for the case of inflow. The no-slip condition is applied for the velocity at all the solid wall boundaries. For the temperature field, all the solid walls are taken as adiabatic except for the ceiling of the shaft, where a convective boundary is imposed

A mesh totalling 100×100 control volumes was generated for the computational domain. Grid sensitivity was performed through refining the mesh to 150×150 control volumes. The computations showed that there was no appreciable difference of the air velocity and temperature with the maximum percentage deviations being less than 1% and 2% respectively.

The algebraic forms of the transport equations were achieved through the finite volume discretisation. In order to reduce the numerical diffusion of the advection terms, the third order accurate QUICK scheme was used to approximate the velocities at the faces of the control volumes except for the turbulent model equations where the Power Law scheme was employed. For the time derivative, the second-order implicit scheme was adopted for computations of the transient solutions. The SIMPLE algorithm was adopted as the pressure-velocity coupling method to ensure mass conservation of the flow system.

3. RESULTS AND DISCUSSIONS

The numerical model was initially validated against the measurements of Mercier and Jaluria [5]. Comparison between the measurements and numerical predictions and parametric analysis were performed for an aspect ratio, A , of 3.0 with the Gr numbers varying between 10^3 and 10^9 , Re numbers varying between 70 and 1000 and Bi numbers at the top surface of the shaft varying between 1 and 100. The temperature difference, ΔT , was maintained at 80°C .

3.1 Comparison with experimental data

Figure 2 illustrates the flow development represented by the vertical velocity profiles at four different heights of $y = 0.167 H$, $0.5 H$, $0.75 H$ and $0.95 H$ for $Bi = 1$, $Re = 75$ and $Gr = 6 \times 10^3$. The model predictions agreed very well with the measurements for all the respective heights along the shaft. Near the inlet, $y = 0.167 H$, the upwards movement of the hot air along the shaft was characterised by steep velocity gradients close to the shaft walls with the appearance of two velocity peaks. Near the outlet, $y = 0.95 H$, the vertical velocity being negative on the right hand side of the shaft wall signified the dilution of the hot air with the cold air entrained into the shaft from the top exhaust. On the opposite side, the hot air travelling upwards along the shaft was indicated by the positive vertical

velocity. In between these heights, the flow of the hot air along the shaft appeared to be in a transitional stage.

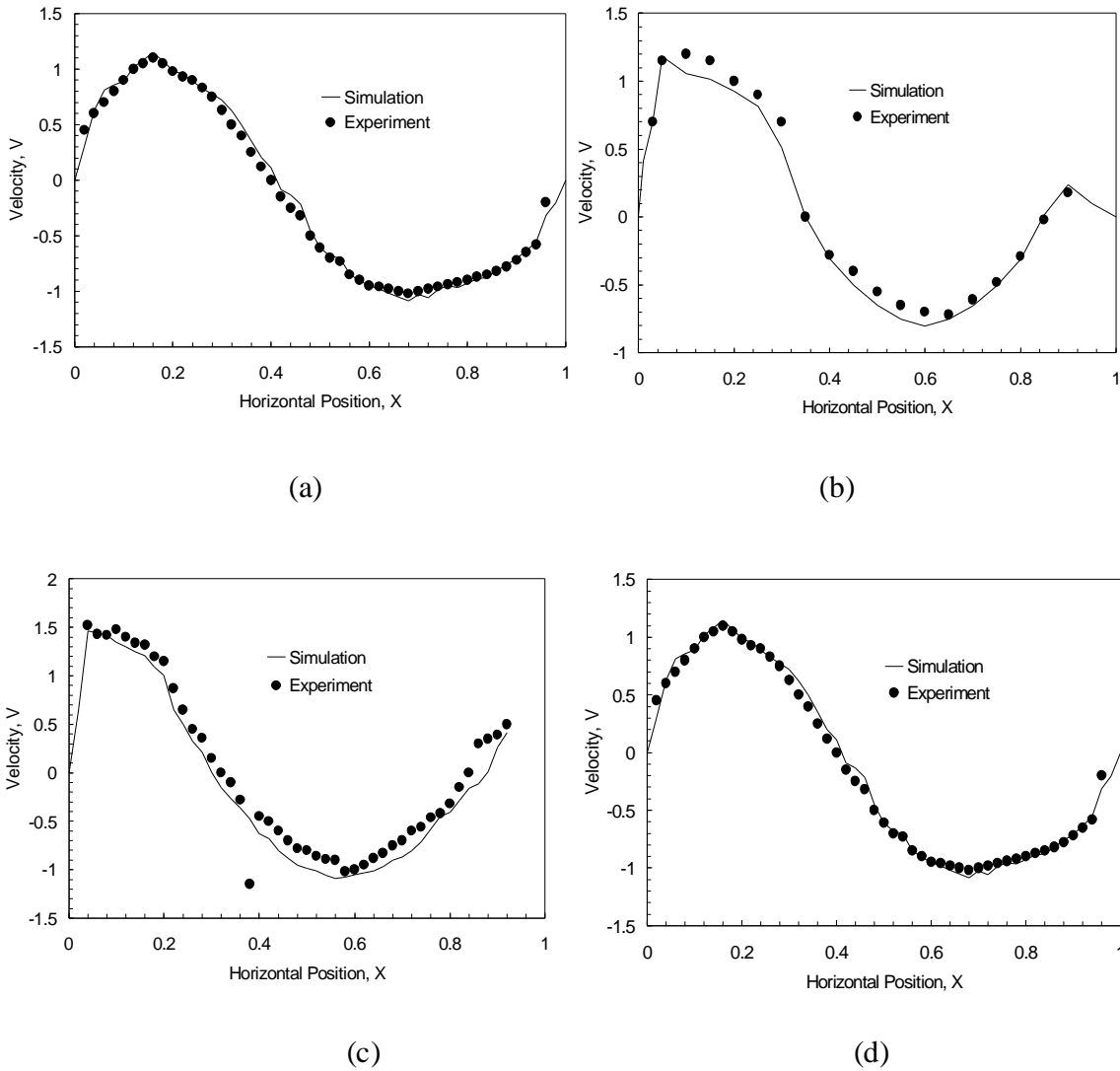


Figure 2 Comparison of simulation and experimental vertical velocity profiles across the shaft for $Re = 75$ and $Gr = 6 \times 10^3$ at different heights: (a) $y = 0.167 H$, (b) $y = 0.5 H$, (c) $y = 0.75 H$ and (d) $y = 0.95 H$.

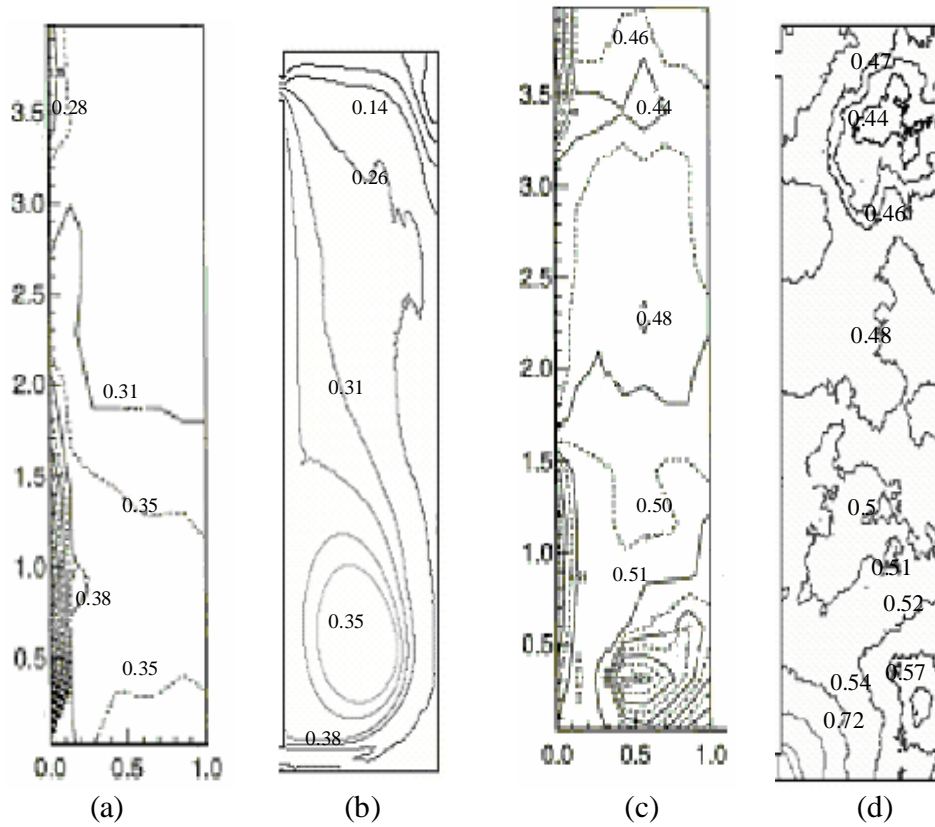


Figure 3 Isotherms of simulations and experiment in the vertical draft for different Re and Gr number: (a) experiment results for $Re = 70$ and $Gr = 6 \times 10^3$, (b) simulation results for $Re = 70$ and $Gr = 6 \times 10^3$, (c) experiment results for $Re = 400$ and $Gr = 6 \times 10^3$ and (d) simulation results for $Re = 400$ and $Gr = 6 \times 10^3$.

Figure 3 presents the comparison between the measured and predicted isotherms at a fixed $Gr = 6 \times 10^3$ for $Re = 70$ and 400 . These results demonstrate the competing modes dominating the fluid motion by either the forced or free convection or a combination of both. For the low Re case, the predicted isotherms were found to be significantly different from the measurements. One possible explanation for the discrepancy could be the adiabatic condition applied for the temperature at the wall surfaces. The buoyancy-driven flow mainly by free convection was allowed to penetrate deeper into the confined space of the shaft since there were no heat losses across the shaft walls. A convective boundary condition, imposed at the top surface of the shaft, could be similarly applied to these walls to halt the strong penetration of the buoyancy-driven flow due to some fraction of the heat escaping into the surroundings. This thereby could make the temperature distribution more comparable to the measurements. Nevertheless, the actual Bi numbers to be employed are not easily known. A sensitivity study of the effect of different Bi numbers was performed on the hot gas temperature at the exhaust outlet, which more details of the investigation are described below. On the contrary, for the higher Re case, the fluid motion driven more by force convection promoted more vigorous mixing of the

hot air with the cold air drawn from the top exhaust. There were still some discrepancies between the predictions and measurements especially near the wall regions but better agreement was achieved especially in the middle region of the shaft.

3.2 Parametric analysis

The vertical velocity and temperature profiles in Figure 4 were obtained by varying the Gr numbers of 10^3 , 10^6 and 10^8 whilst fixing the Re number to be 100. In Figure 5, however, the results were represented by varying the Re numbers of 100, 500 and 1000 for a fixed Gr number at 10^6 . This parametric investigation aimed to determine the extent of the free or forced convection modes affecting the buoyancy-driven flow behaviour of the hot gas. All the above profiles were plotted at the mid-height of the shaft, i.e. at $y = 0.5 H$. In general, the flow and heat characteristics were rather similar when the fluid motion was agitated by either increasing the Re or Gr numbers. For the bounding cases in Figures 4 and 5, the maximum values of the vertical velocity, whether positive (upward flow) on the left hand side of the shaft or negative (downward flow) on the opposite side, were only marginally higher for the case of high Re number in comparison to the case of high Gr number. The temperatures for the case of increasing Re numbers at a fixed Gr number were found to follow the similar trend illustrated by the vertical velocity profiles. At high Re number, the gas temperatures were found to be closed to the inlet temperature. However, the temperatures showed the reverse trend for the case of increasing Gr numbers at a fixed Re number where they were significantly lower at high Gr number because of the vigorous mixing promoted between the incoming hot air from the inlet and the cold air being entrained from the top exhaust. This indicated a complex flow structure represented by the presence of recirculation convective cells.

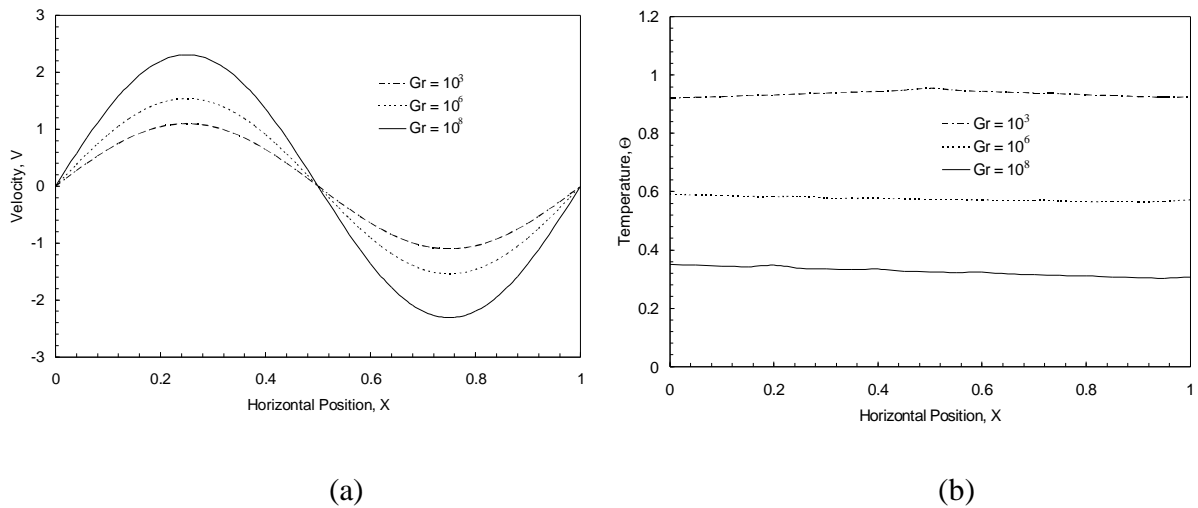


Figure 4 Simulation results for $Re = 100$ and $Gr = 10^3, 10^6$ and 10^8 across the shaft horizontal distance at $y = H/2$: (a) Vertical velocity and (b) Temperature

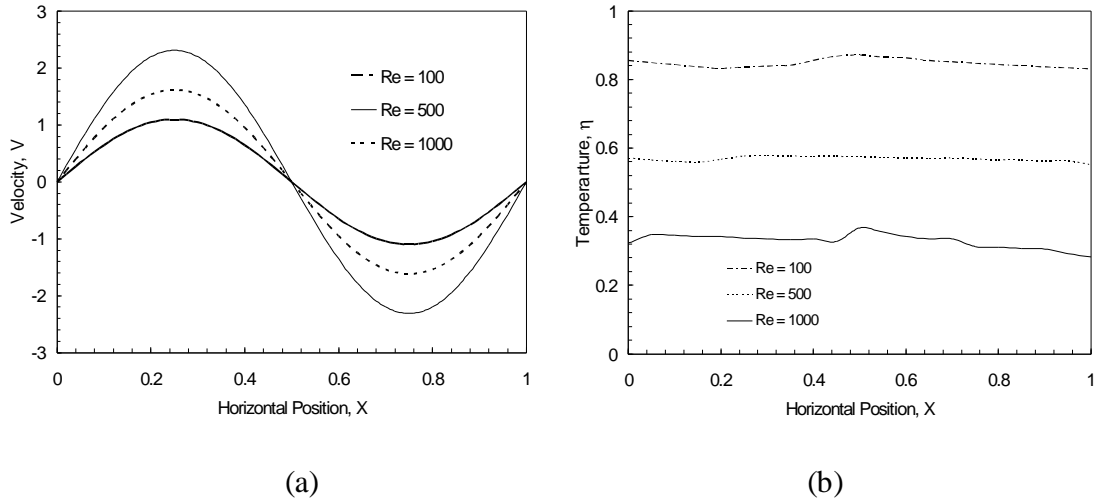


Figure 5 Simulation results for $Gr = 10^6$ and $Re = 100, 500$ and 1000 across the shaft at $y = H/2$: (a) Vertical velocity and (b) Temperature.

Thus far, the analysis has only concentrated on the fire-induced flow at laminar conditions because of the reduced-scaling of the model being solved. In a full-scale fire scenario, the Gr and Re numbers would easily lie in the turbulent regime because of the large scaling associated to an actual building structure in comparison to those of the reduced-scale model. Figures 6 and 7 illustrate the comparison of the flow behaviour by the predicted streamlines and isotherms at laminar and turbulent conditions. For laminar flow, where the Re and Gr numbers are low, the streamlines revealed a uniform flow near the inlet and top exhaust regions. However, as the hot air entered the shaft, the streamlines indicated a recirculating cell driven by the buoyancy forces in the core region of the shaft. The flow structure also revealed very thin boundary layer flows along the vertical adiabatic shaft walls. For turbulent flow, at high Re and Gr numbers, because of the vigorous mixing promoted by the energetic turbulent eddies, the fluid flow and heat transfer were found to be more evenly distributed throughout the core region of the shaft. The streamlines looked rather symmetry about the mid-height plane of the shaft. For the isotherms when the Gr number is small, the variations in the middle and outlet were small. However, multi-cells being present in the middle and outlet of the shaft at high Gr number revealed strong localized recirculation buoyant-induced turbulent flows that promoted cooling of the hot air from the inlet and heating of the cold air drawn from the top exhaust.

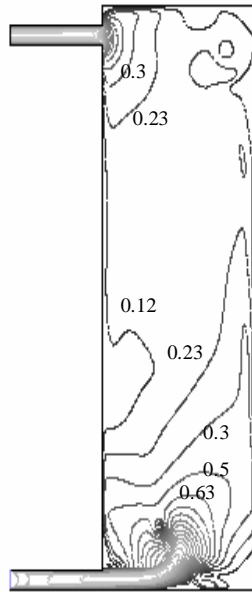


Figure 7(a)

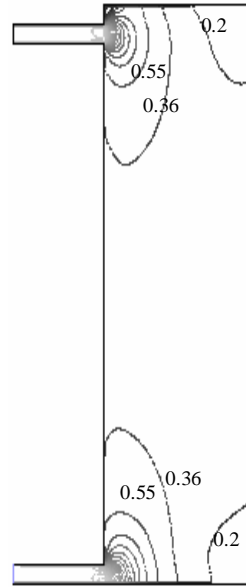


Figure 7(b)

Figure 6 Simulated streamlines: (a) laminar condition – $Re = 70$ and $Gr = 10^3$ and (b) turbulent condition – $Re = 1000$ and $Gr = 10^9$.

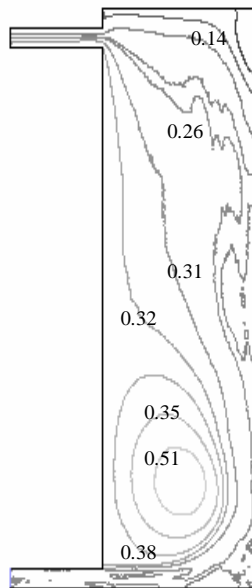


Figure 8(a)

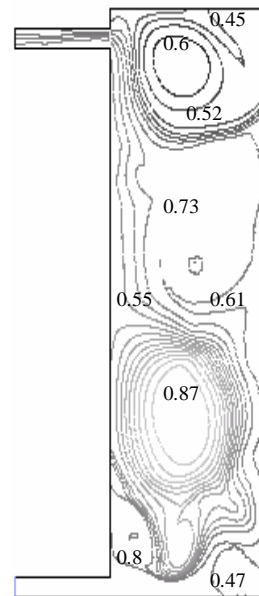


Figure 8(b)

Figure 7 Simulated isotherms: (a) laminar condition – $Re = 70$ and $Gr = 10^3$ and (b) turbulent condition – $Re = 1000$ and $Gr = 10^9$.

4. CONCLUSIONS

The fire-induced flow in a vertical shaft has been numerically simulated. The results were validated against the experimental data of Mercier and Jaluria [9]. Good agreement was achieved between the predictions and measurements. When the Gr number or Re number was low, a wall plume of hot gases could be seen developing in the interior region of the vertical shaft. However, when the Gr number or Re number was high, the flow structure was represented by a thin boundary layer along the wall with a large recirculating convective cell. The velocity field was found to be similar when the Gr number or Re number was varied but the temperature field behaved otherwise in particular the temperatures showed the reverse trend for the case of increasing Gr numbers at a fixed Re number.

REFERENCES

1. H. W. Emmons, The Prediction of Fire in Buildings, *9th Symposium (International) on Combustion*, Combustion Institute, pp. 1101-1110, 1987.
2. J. Cannon and E. Zukoski, Turbulent Mixing in Vertical Shafts Under Conditions Applicable to Fires in High Rise Buildings, Internal Report, California Institute of Technology, CA, 1976.
3. J. G. Quintiere, Perspective on Compartment Fire Growth, *Comb. Sci. Tech.*, vol. 39, pp. 11-54, 1984
4. S. Y. Kim and Y. Jaluria, Basic Considerations in Combined Buoyancy-Induced and Forced Flow in a Vertical Open Shaft, *Num. Heat Transfer*, Vol. 34, pp. 519-536, 1998.
5. G. P. Mercier and Y. Jaluria, Fire-Induced Flow of Smoke and Hot Gases in Open Vertical Shafts, *Exp. Thermal Fluid Sci.*, vol. 13, pp. 77-84, 1999.
6. E. Launder and D. B. Spalding, The Numerical Computation of Turbulent Flows, *Comp. Meth. Appl. Mech. & Eng.*, vol. 3, pp 269-289, 1974.
7. FLUENT, version 6.0, *Computational Fluid Dynamics User's Guide manual*, Hanover, New Hampshire, 2001.
8. A. A. Mohamad, Natural Convection in Open Cavities and Slots, *Num. Heat Transfer*, vol. 27, pp. 705-716, 1995.

CFD prediction of fire-induced hot gases in buildings

G.Q. Xiao^{1,2}, J.Y. Tu¹, G.H. Yeoh³

Abstract

A CFD model was developed to predict the fire-induced hot gas within internal narrow passages in enclosures in buildings, such as elevator shafts in buildings. Simulations were performed to predict the spatial variation of temperature and velocity distributions in this configuration. The computational results were compared against the experiments of Mercier and Jaluria (1999). Good agreement was achieved between the experimental data and model predictions. The results obtained indicated that the primary transport mechanism affecting the temperature and velocity distributions within the internal passage was due to the buoyancy effect caused by temperature difference of the airflow. In the results, a thin boundary layer was formed along the vertical wall as the Grashof number was increased while the Reynolds number was kept fixed, and the recirculation of the airflow became more pronounced in the flow field.

¹ School of Aerospace, Mechanical and Manufacturing Engineering, RMIT University, Victoria 3083, Australia

² School of Energy and Safety Engineering, Hunan University of Science and Technology, Xiangtan, Hunan, 411201, China

³ Australian Nuclear Science and Technology Organization (ANSTO), PMB 1, Menai, NSW 2234, Australia

1. INTRODUCTION

The building fire can cause considerable damage to building structures and human lives[1,2]; the principal hazard in fire is usually the spread of sooty smoke and hot toxic gas which can flow through vents, openings and internal passages such as ventilation ducts, stairwells, and elevator shafts, Although a large amount of results has been reported concerning fires in enclosures such as offices and rooms, little attention has been given to investigate fire-induced gas flows in modern high-rise buildings. Concerning the possibilities of these many flow-paths, the spilling of hot smoke and toxic gases in an open shaft of a multistorey building is investigated herein because of the imposing hazardous condition.

One possible way of studying this problem could involve a full-scale instrumentation of a building structure [3]. Nevertheless, such an approach may not deem to be feasible because of the high costs associated with construction and the demanding resources of instrumentation. With the advancements of computer resources and speeds, and rapid developments of numerical methodologies, numerical models are becoming increasingly powerful to study such problem. Despite the efforts of Kim and Jaluria [4] where they have developed a numerical model to solve the laminar flow in a large aspect ratio shaft, there have not been many comparisons with measurements. The lack of attention may be attributed to the complexity of the flow being vigorously turbulent that will significantly affect the fluid flow and heat transfer characteristics in a full-scale structure. As a result, no comparison exists between measurements and numerical models for turbulent flows.

In this paper, the application a computational fluid dynamics (CFD) model is evaluated for the fire-induced flow in a vertical shaft in buildings. Figure 1 describes the schematic configuration of the vertical model shaft. The width and height of the shaft are

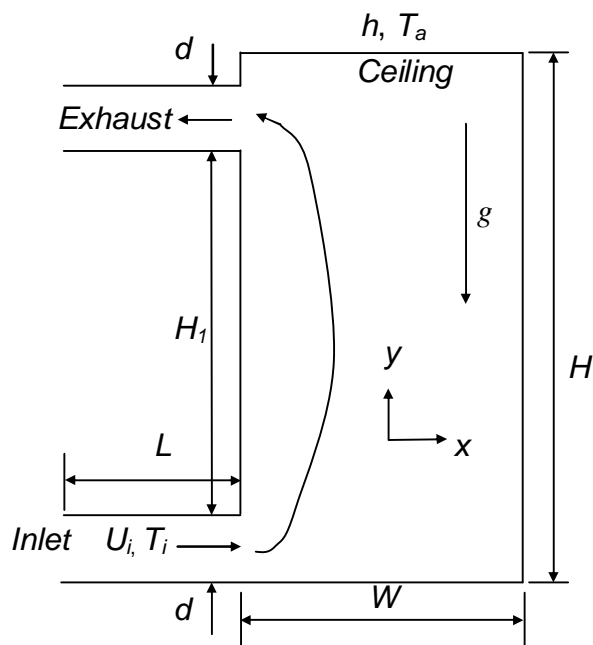


Figure 1 Schematic drawing of the vertical shaft configuration

0.5 m and 1.5 m while the height and length of inlet and outlet are 0.05 m and 0.3 m respectively. The distance between the outlet and the ceiling of the shaft is 0.1 m. The calculated air flow velocities and temperatures of the model in laminar conditions are simulated and verified against the experiment data obtained by Mercier and Jaluria [5]. A parametric investigation is performed on the velocity and temperature fields by varying the Grashof (Gr) number or Reynolds (Re) number. For the case of turbulent flow, the standard two-equation k - ϵ turbulent model [6] is employed and the predicted flow fields are compared against those in laminar conditions.

2. COMPUTATIONAL MODELS

A generic CFD commercial code, FLUENT [7], is utilised to predict the continuum gas phase of the velocity and temperature profiles under unsteady and incompressible conditions through solutions to the conservation of mass, momentum and energy. The buoyancy force due to gravity is accounted by invoking the Boussinesq approximation in the momentum equation. A two-dimensional model is adopted for the current simulation. The governing equations under consideration can be written in non-dimensional form as:

$$\frac{\partial U}{\partial X} + \frac{\partial V}{\partial Y} = 0 \quad (1)$$

$$\frac{\partial U}{\partial t_c} + \frac{\partial(UU)}{\partial X} + \frac{\partial(UV)}{\partial Y} = -\frac{\partial P}{\partial X} + \left\{ \frac{1}{Re} + \frac{1}{Re_t} \right\} \left(\frac{\partial^2 U}{\partial X^2} + \frac{\partial^2 U}{\partial Y^2} \right) \quad (2)$$

$$\frac{\partial V}{\partial t_c} + \frac{\partial(UV)}{\partial X} + \frac{\partial(VV)}{\partial Y} = -\frac{\partial P}{\partial Y} + \left\{ \frac{1}{Re} + \frac{1}{Re_t} \right\} \left(\frac{\partial^2 V}{\partial X^2} + \frac{\partial^2 V}{\partial Y^2} \right) + \frac{Gr}{Re^2} \Theta \quad (3)$$

$$\frac{\partial \Theta}{\partial t_c} + \frac{\partial(U\Theta)}{\partial X} + \frac{\partial(V\Theta)}{\partial Y} = \left\{ \frac{1}{Pe} + \frac{1}{Pe_t} \right\} \left(\frac{\partial^2 \Theta}{\partial X^2} + \frac{\partial^2 \Theta}{\partial Y^2} \right) \quad (4)$$

The following non-dimensional variables are given by:

$$X = \frac{x}{H}; \quad Y = \frac{y}{H}; \quad U = \frac{u}{U_i}; \quad V = \frac{v}{U_i}; \quad P = \frac{P}{\rho U_i^2}; \quad \tau_c = \frac{t}{H/U_i}; \quad \Theta = \frac{T - T_a}{\Delta T}$$

where the lower-case letters denote the dimensional variables. The velocity components u and v correspond to the x and y directions of the Cartesian coordinate system while the dimensionless time t_c is defined as the convective timescale. The non-dimensional parameters in the above equations are defined as: the laminar and turbulent Reynolds numbers – $Re = U_i H / \nu$ and $Re_t = U_i H / \nu_t$; the Grashof number – $g b \Delta T H^3 / \nu^2$; and the laminar and turbulent Péclet numbers – $Pe = Re Pr$ and $Pe_t = Re_t Pr_t$. The kinematic viscosity of the fluid is denoted by ν , the coefficient of volumetric expansion by b and the temperature difference between the temperatures at the inlet and ambient condition by $\Delta T = (T_i - T_a)$.

For laminar flow, the turbulent Reynolds and Péclet numbers diminish in the momentum and energy equations. Nevertheless, for turbulent flow, the eddy-viscosity concept is employed for the representation of the turbulent Reynolds and Péclet numbers in the governing equations due to turbulence. This is expressed by the solution of the standard k - ϵ turbulent model with additional source terms to account for buoyancy effects. At the inlet, a uniform unidirectional velocity U_i and temperature T_i are prescribed, the outlet conditions that involve setting the continuity equation and relative pressure to be zero at the top exhaust boundary[8] (see Figure 1). Neumann condition is imposed for the case of outflow while Dirichlet condition is applied for the case of inflow. The no-slip condition is applied for the velocity at all the solid wall boundaries. For the temperature field, all the solid walls are taken as adiabatic except for the ceiling of the shaft, where a convective boundary is imposed

A mesh totalling 100×100 control volumes was generated for the computational domain. Grid sensitivity was performed through refining the mesh to 150×150 control volumes. The computations showed that there was no appreciable difference of the air velocity and temperature with the maximum percentage deviations being less than 1% and 2% respectively.

The algebraic forms of the transport equations were achieved through the finite volume discretisation. In order to reduce the numerical diffusion of the advection terms, the third order accurate QUICK scheme was used to approximate the velocities at the faces of the control volumes except for the turbulent model equations where the Power Law scheme was employed. For the time derivative, the second-order implicit scheme was adopted for computations of the transient solutions. The SIMPLE algorithm was adopted as the pressure-velocity coupling method to ensure mass conservation of the flow system.

3. RESULTS AND DISCUSSIONS

The numerical model was initially validated against the measurements of Mercier and Jaluria [5]. Comparison between the measurements and numerical predictions and parametric analysis were performed for an aspect ratio, A , of 3.0 with the Gr numbers varying between 10^3 and 10^9 , Re numbers varying between 70 and 1000 and Bi numbers at the top surface of the shaft varying between 1 and 100. The temperature difference, ΔT , was maintained at 80°C .

3.1 Comparison with experimental data

Figure 2 illustrates the flow development represented by the vertical velocity profiles at four different heights of $y = 0.167 H$, $0.5 H$, $0.75 H$ and $0.95 H$ for $Bi = 1$, $Re = 75$ and $Gr = 6 \times 10^3$. The model predictions agreed very well with the measurements for all the respective heights along the shaft. Near the inlet, $y = 0.167 H$, the upwards movement of the hot air along the shaft was characterised by steep velocity gradients close to the shaft walls with the appearance of two velocity peaks. Near the outlet, $y = 0.95 H$, the vertical velocity being negative on the right hand side of the shaft wall signified the dilution of the hot air with the cold air entrained into the shaft from the top exhaust. On the opposite side, the hot air travelling upwards along the shaft was indicated by the positive vertical

velocity. In between these heights, the flow of the hot air along the shaft appeared to be in a transitional stage.

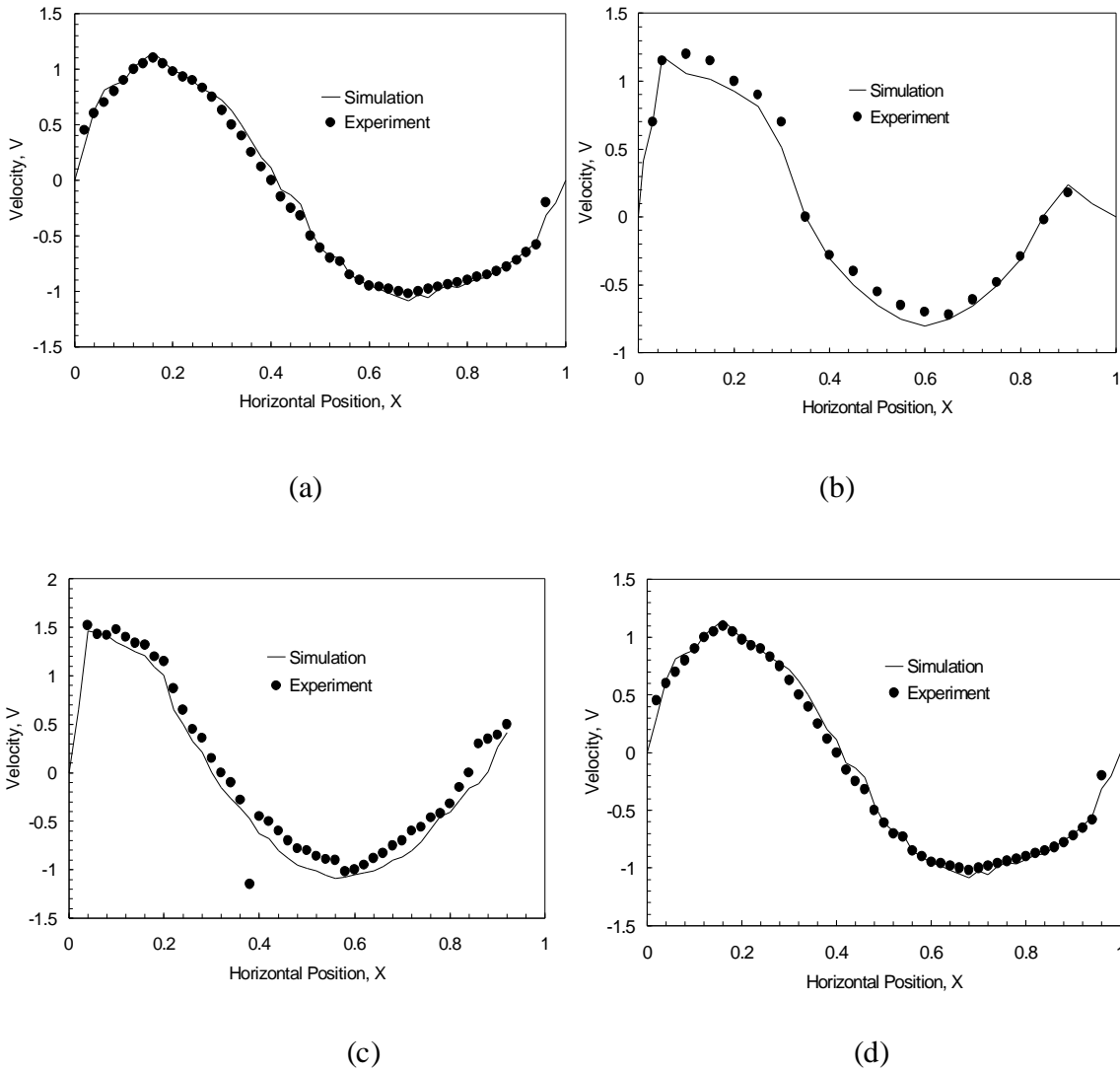


Figure 2 Comparison of simulation and experimental vertical velocity profiles across the shaft for $Re = 75$ and $Gr = 6 \times 10^3$ at different heights: (a) $y = 0.167 H$, (b) $y = 0.5 H$, (c) $y = 0.75 H$ and (d) $y = 0.95 H$.

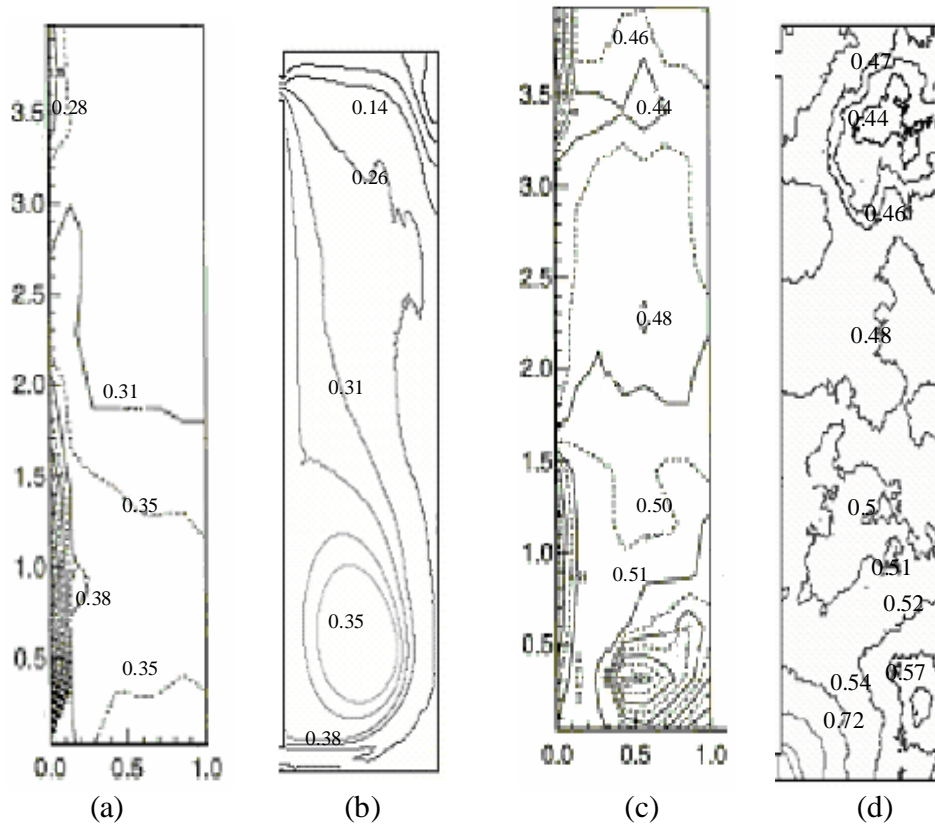


Figure 3 Isotherms of simulations and experiment in the vertical draft for different Re and Gr number: (a) experiment results for $Re = 70$ and $Gr = 6 \times 10^3$, (b) simulation results for $Re = 70$ and $Gr = 6 \times 10^3$, (c) experiment results for $Re = 400$ and $Gr = 6 \times 10^3$ and (d) simulation results for $Re = 400$ and $Gr = 6 \times 10^3$.

Figure 3 presents the comparison between the measured and predicted isotherms at a fixed $Gr = 6 \times 10^3$ for $Re = 70$ and 400 . These results demonstrate the competing modes dominating the fluid motion by either the forced or free convection or a combination of both. For the low Re case, the predicted isotherms were found to be significantly different from the measurements. One possible explanation for the discrepancy could be the adiabatic condition applied for the temperature at the wall surfaces. The buoyancy-driven flow mainly by free convection was allowed to penetrate deeper into the confined space of the shaft since there were no heat losses across the shaft walls. A convective boundary condition, imposed at the top surface of the shaft, could be similarly applied to these walls to halt the strong penetration of the buoyancy-driven flow due to some fraction of the heat escaping into the surroundings. This thereby could make the temperature distribution more comparable to the measurements. Nevertheless, the actual Bi numbers to be employed are not easily known. A sensitivity study of the effect of different Bi numbers was performed on the hot gas temperature at the exhaust outlet, which more details of the investigation are described below. On the contrary, for the higher Re case, the fluid motion driven more by force convection promoted more vigorous mixing of the

hot air with the cold air drawn from the top exhaust. There were still some discrepancies between the predictions and measurements especially near the wall regions but better agreement was achieved especially in the middle region of the shaft.

3.2 Parametric analysis

The vertical velocity and temperature profiles in Figure 4 were obtained by varying the Gr numbers of 10^3 , 10^6 and 10^8 whilst fixing the Re number to be 100. In Figure 5, however, the results were represented by varying the Re numbers of 100, 500 and 1000 for a fixed Gr number at 10^6 . This parametric investigation aimed to determine the extent of the free or forced convection modes affecting the buoyancy-driven flow behaviour of the hot gas. All the above profiles were plotted at the mid-height of the shaft, i.e. at $y = 0.5 H$. In general, the flow and heat characteristics were rather similar when the fluid motion was agitated by either increasing the Re or Gr numbers. For the bounding cases in Figures 4 and 5, the maximum values of the vertical velocity, whether positive (upward flow) on the left hand side of the shaft or negative (downward flow) on the opposite side, were only marginally higher for the case of high Re number in comparison to the case of high Gr number. The temperatures for the case of increasing Re numbers at a fixed Gr number were found to follow the similar trend illustrated by the vertical velocity profiles. At high Re number, the gas temperatures were found to be closed to the inlet temperature. However, the temperatures showed the reverse trend for the case of increasing Gr numbers at a fixed Re number where they were significantly lower at high Gr number because of the vigorous mixing promoted between the incoming hot air from the inlet and the cold air being entrained from the top exhaust. This indicated a complex flow structure represented by the presence of recirculation convective cells.

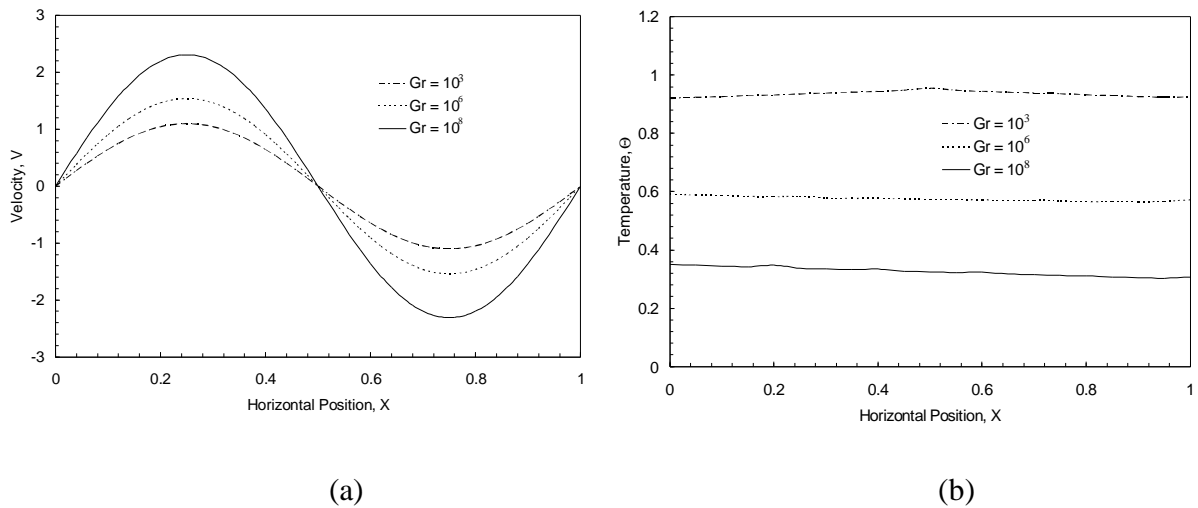


Figure 4 Simulation results for $Re = 100$ and $Gr = 10^3, 10^6$ and 10^8 across the shaft horizontal distance at $y = H/2$: (a) Vertical velocity and (b) Temperature

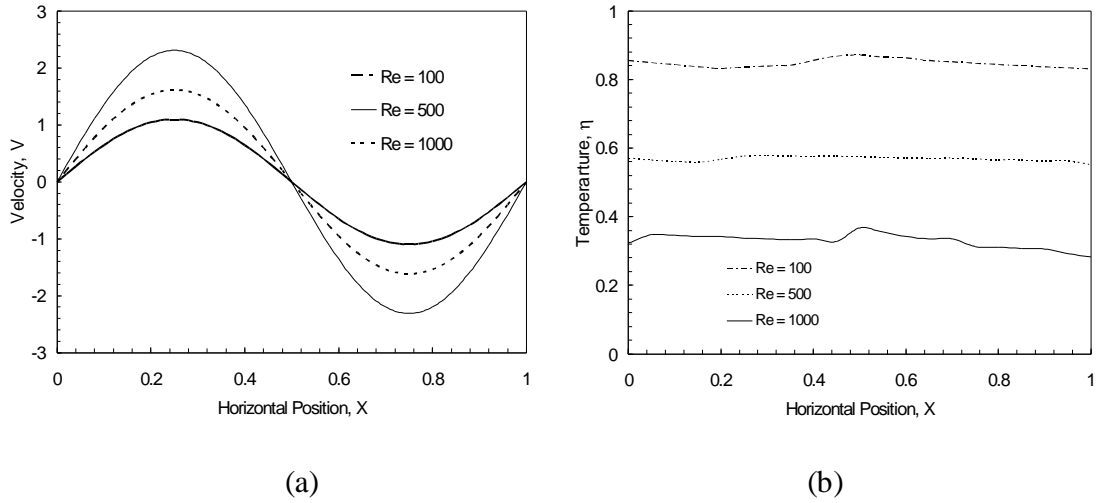


Figure 5 Simulation results for $Gr = 10^6$ and $Re = 100, 500$ and 1000 across the shaft at $y = H/2$: (a) Vertical velocity and (b) Temperature.

Thus far, the analysis has only concentrated on the fire-induced flow at laminar conditions because of the reduced-scaling of the model being solved. In a full-scale fire scenario, the Gr and Re numbers would easily lie in the turbulent regime because of the large scaling associated to an actual building structure in comparison to those of the reduced-scale model. Figures 6 and 7 illustrate the comparison of the flow behaviour by the predicted streamlines and isotherms at laminar and turbulent conditions. For laminar flow, where the Re and Gr numbers are low, the streamlines revealed a uniform flow near the inlet and top exhaust regions. However, as the hot air entered the shaft, the streamlines indicated a recirculating cell driven by the buoyancy forces in the core region of the shaft. The flow structure also revealed very thin boundary layer flows along the vertical adiabatic shaft walls. For turbulent flow, at high Re and Gr numbers, because of the vigorous mixing promoted by the energetic turbulent eddies, the fluid flow and heat transfer were found to be more evenly distributed throughout the core region of the shaft. The streamlines looked rather symmetry about the mid-height plane of the shaft. For the isotherms when the Gr number is small, the variations in the middle and outlet were small. However, multi-cells being present in the middle and outlet of the shaft at high Gr number revealed strong localized recirculation buoyant-induced turbulent flows that promoted cooling of the hot air from the inlet and heating of the cold air drawn from the top exhaust.

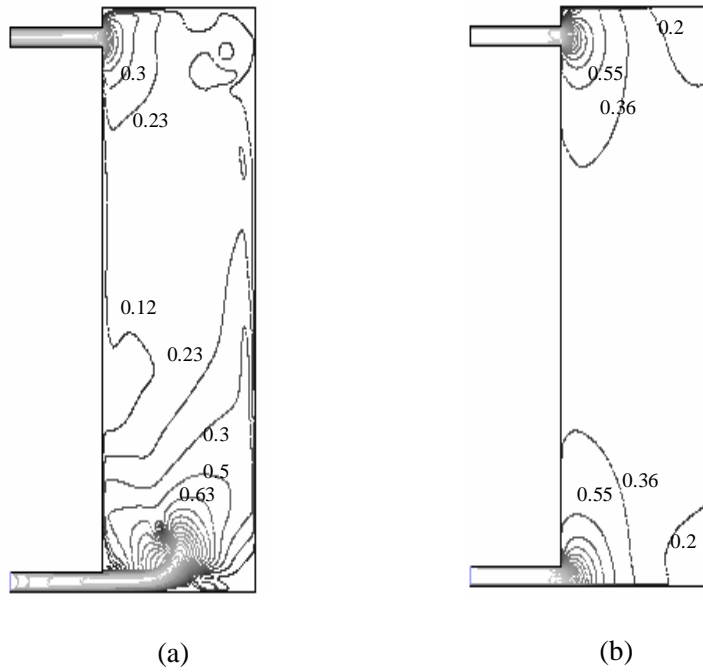


Figure 6 Simulated streamlines: (a) laminar condition – $Re = 70$ and $Gr = 10^3$ and (b) turbulent condition – $Re = 1000$ and $Gr = 10^9$.

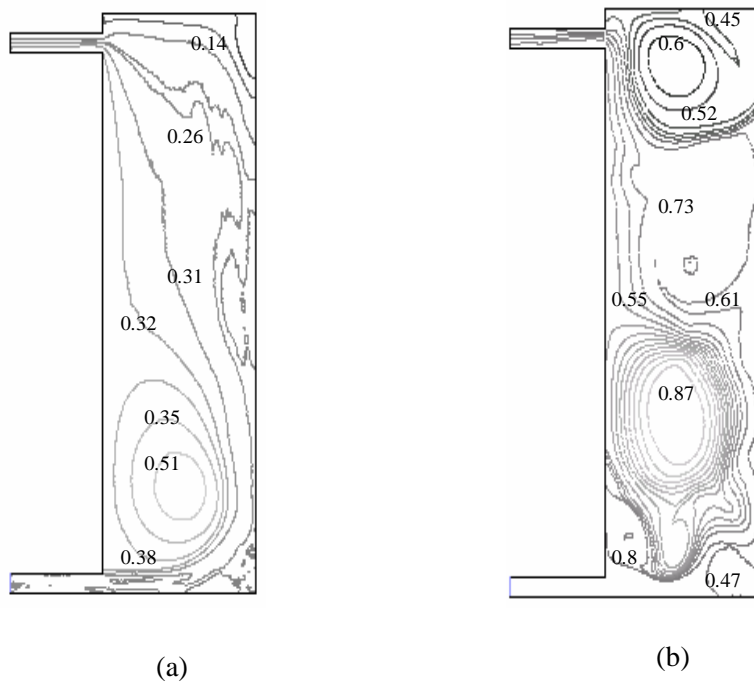


Figure 7 Simulated isotherms: (a) laminar condition – $Re = 70$ and $Gr = 10^3$ and (b) turbulent condition – $Re = 1000$ and $Gr = 10^9$.

4. CONCLUSIONS

The fire-induced flow in a vertical shaft has been numerically simulated. The results were validated against the experimental data of Mercier and Jaluria [9]. Good agreement was achieved between the predictions and measurements. When the Gr number or Re number was low, a wall plume of hot gases could be seen developing in the interior region of the vertical shaft. However, when the Gr number or Re number was high, the flow structure was represented by a thin boundary layer along the wall with a large recirculating convective cell. The velocity field was found to be similar when the Gr number or Re number was varied but the temperature field behaved otherwise in particular the temperatures showed the reverse trend for the case of increasing Gr numbers at a fixed Re number.

REFERENCES

1. H. W. Emmons, The Prediction of Fire in Buildings, *9th Symposium (International) on Combustion*, Combustion Institute, pp. 1101-1110, 1987.
2. J. Cannon and E. Zukoski, Turbulent Mixing in Vertical Shafts Under Conditions Applicable to Fires in High Rise Buildings, Internal Report, California Institute of Technology, CA, 1976.
3. J. G. Quintiere, Perspective on Compartment Fire Growth, *Comb. Sci. Tech.*, vol. 39, pp. 11-54, 1984
4. S. Y. Kim and Y. Jaluria, Basic Considerations in Combined Buoyancy-Induced and Forced Flow in a Vertical Open Shaft, *Num. Heat Transfer*, Vol. 34, pp. 519-536, 1998.
5. G. P. Mercier and Y. Jaluria, Fire-Induced Flow of Smoke and Hot Gases in Open Vertical Shafts, *Exp. Thermal Fluid Sci.*, vol. 13, pp. 77-84, 1999.
6. E. Launder and D. B. Spalding, The Numerical Computation of Turbulent Flows, *Comp. Meth. Appl. Mech. & Eng.*, vol. 3, pp 269-289, 1974.
7. FLUENT, version 6.0, *Computational Fluid Dynamics User's Guide manual*, Hanover, New Hampshire, 2001.
8. A. A. Mohamad, Natural Convection in Open Cavities and Slots, *Num. Heat Transfer*, vol. 27, pp. 705-716, 1995.

CFD prediction of fire-induced hot gases in buildings

G.Q. Xiao^{1,2}, J.Y. Tu¹, G.H. Yeoh³

Abstract

A CFD model was developed to predict the fire-induced hot gas within internal narrow passages in enclosures in buildings, such as elevator shafts in buildings. Simulations were performed to predict the spatial variation of temperature and velocity distributions in this configuration. The computational results were compared against the experiments of Mercier and Jaluria (1999). Good agreement was achieved between the experimental data and model predictions. The results obtained indicated that the primary transport mechanism affecting the temperature and velocity distributions within the internal passage was due to the buoyancy effect caused by temperature difference of the airflow. In the results, a thin boundary layer was formed along the vertical wall as the Grashof number was increased while the Reynolds number was kept fixed, and the recirculation of the airflow became more pronounced in the flow field.

¹ School of Aerospace, Mechanical and Manufacturing Engineering, RMIT University, Victoria 3083, Australia

² School of Energy and Safety Engineering, Hunan University of Science and Technology, Xiangtan, Hunan, 411201, China

³ Australian Nuclear Science and Technology Organization (ANSTO), PMB 1, Menai, NSW 2234, Australia

1. INTRODUCTION

The building fire can cause considerable damage to building structures and human lives[1,2]; the principal hazard in fire is usually the spread of sooty smoke and hot toxic gas which can flow through vents, openings and internal passages such as ventilation ducts, stairwells, and elevator shafts, Although a large amount of results has been reported concerning fires in enclosures such as offices and rooms, little attention has been given to investigate fire-induced gas flows in modern high-rise buildings. Concerning the possibilities of these many flow-paths, the spilling of hot smoke and toxic gases in an open shaft of a multistorey building is investigated herein because of the imposing hazardous condition.

One possible way of studying this problem could involve a full-scale instrumentation of a building structure [3]. Nevertheless, such an approach may not deem to be feasible because of the high costs associated with construction and the demanding resources of instrumentation. With the advancements of computer resources and speeds, and rapid developments of numerical methodologies, numerical models are becoming increasingly powerful to study such problem. Despite the efforts of Kim and Jaluria [4] where they have developed a numerical model to solve the laminar flow in a large aspect ratio shaft, there have not been many comparisons with measurements. The lack of attention may be attributed to the complexity of the flow being vigorously turbulent that will significantly affect the fluid flow and heat transfer characteristics in a full-scale structure. As a result, no comparison exists between measurements and numerical models for turbulent flows.

In this paper, the application a computational fluid dynamics (CFD) model is evaluated for the fire-induced flow in a vertical shaft in buildings. Figure 1 describes the schematic configuration of the vertical model shaft. The width and height of the shaft are

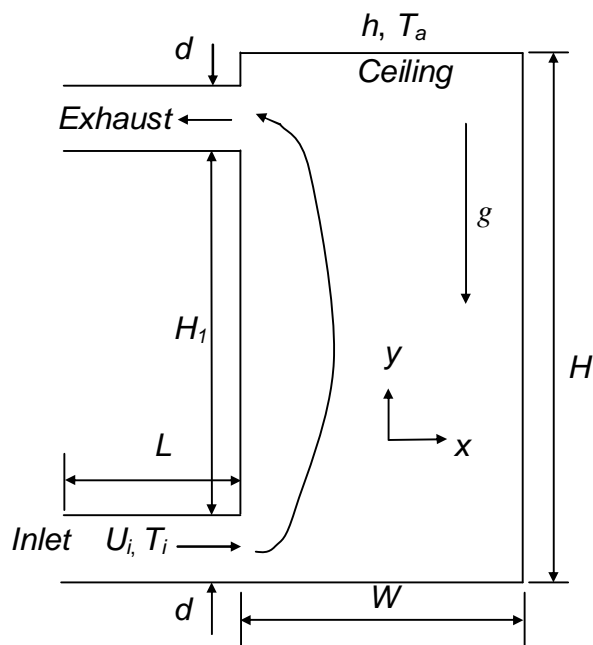


Figure 1 Schematic drawing of the vertical shaft configuration

0.5 m and 1.5 m while the height and length of inlet and outlet are 0.05 m and 0.3 m respectively. The distance between the outlet and the ceiling of the shaft is 0.1 m. The calculated air flow velocities and temperatures of the model in laminar conditions are simulated and verified against the experiment data obtained by Mercier and Jaluria [5]. A parametric investigation is performed on the velocity and temperature fields by varying the Grashof (Gr) number or Reynolds (Re) number. For the case of turbulent flow, the standard two-equation k - ϵ turbulent model [6] is employed and the predicted flow fields are compared against those in laminar conditions.

2. COMPUTATIONAL MODELS

A generic CFD commercial code, FLUENT [7], is utilised to predict the continuum gas phase of the velocity and temperature profiles under unsteady and incompressible conditions through solutions to the conservation of mass, momentum and energy. The buoyancy force due to gravity is accounted by invoking the Boussinesq approximation in the momentum equation. A two-dimensional model is adopted for the current simulation. The governing equations under consideration can be written in non-dimensional form as:

$$\frac{\partial U}{\partial X} + \frac{\partial V}{\partial Y} = 0 \quad (1)$$

$$\frac{\partial U}{\partial t_c} + \frac{\partial(UU)}{\partial X} + \frac{\partial(UV)}{\partial Y} = -\frac{\partial P}{\partial X} + \left\{ \frac{1}{Re} + \frac{1}{Re_t} \right\} \left(\frac{\partial^2 U}{\partial X^2} + \frac{\partial^2 U}{\partial Y^2} \right) \quad (2)$$

$$\frac{\partial V}{\partial t_c} + \frac{\partial(UV)}{\partial X} + \frac{\partial(VV)}{\partial Y} = -\frac{\partial P}{\partial Y} + \left\{ \frac{1}{Re} + \frac{1}{Re_t} \right\} \left(\frac{\partial^2 V}{\partial X^2} + \frac{\partial^2 V}{\partial Y^2} \right) + \frac{Gr}{Re^2} \Theta \quad (3)$$

$$\frac{\partial \Theta}{\partial t_c} + \frac{\partial(U\Theta)}{\partial X} + \frac{\partial(V\Theta)}{\partial Y} = \left\{ \frac{1}{Pe} + \frac{1}{Pe_t} \right\} \left(\frac{\partial^2 \Theta}{\partial X^2} + \frac{\partial^2 \Theta}{\partial Y^2} \right) \quad (4)$$

The following non-dimensional variables are given by:

$$X = \frac{x}{H}; \quad Y = \frac{y}{H}; \quad U = \frac{u}{U_i}; \quad V = \frac{v}{U_i}; \quad P = \frac{P}{\rho U_i^2}; \quad \tau_c = \frac{t}{H/U_i}; \quad \Theta = \frac{T - T_a}{\Delta T}$$

where the lower-case letters denote the dimensional variables. The velocity components u and v correspond to the x and y directions of the Cartesian coordinate system while the dimensionless time t_c is defined as the convective timescale. The non-dimensional parameters in the above equations are defined as: the laminar and turbulent Reynolds numbers – $Re = U_i H / \nu$ and $Re_t = U_i H / \nu_t$; the Grashof number – $g b \Delta T H^3 / \nu^2$; and the laminar and turbulent Péclet numbers – $Pe = Re Pr$ and $Pe_t = Re_t Pr_t$. The kinematic viscosity of the fluid is denoted by ν , the coefficient of volumetric expansion by b and the temperature difference between the temperatures at the inlet and ambient condition by $\Delta T = (T_i - T_a)$.

For laminar flow, the turbulent Reynolds and Péclet numbers diminish in the momentum and energy equations. Nevertheless, for turbulent flow, the eddy-viscosity concept is employed for the representation of the turbulent Reynolds and Péclet numbers in the governing equations due to turbulence. This is expressed by the solution of the standard k - ϵ turbulent model with additional source terms to account for buoyancy effects. At the inlet, a uniform unidirectional velocity U_i and temperature T_i are prescribed, the outlet conditions that involve setting the continuity equation and relative pressure to be zero at the top exhaust boundary[8] (see Figure 1). Neumann condition is imposed for the case of outflow while Dirichlet condition is applied for the case of inflow. The no-slip condition is applied for the velocity at all the solid wall boundaries. For the temperature field, all the solid walls are taken as adiabatic expect for the ceiling of the shaft, where a convective boundary is imposed

A mesh totalling 100×100 control volumes was generated for the computational domain. Grid sensitivity was performed through refining the mesh to 150×150 control volumes. The computations showed that there was no appreciable difference of the air velocity and temperature with the maximum percentage deviations being less than 1% and 2% respectively.

The algebraic forms of the transport equations were achieved through the finite volume discretisation. In order to reduce the numerical diffusion of the advection terms, the third order accurate QUICK scheme was used to approximate the velocities at the faces of the control volumes except for the turbulent model equations where the Power Law scheme was employed. For the time derivative, the second-order implicit scheme was adopted for computations of the transient solutions. The SIMPLE algorithm was adopted as the pressure-velocity coupling method to ensure mass conservation of the flow system.

3. RESULTS AND DISCUSSIONS

The numerical model was initially validated against the measurements of Mercier and Jaluria [5]. Comparison between the measurements and numerical predictions and parametric analysis were performed for an aspect ratio, A , of 3.0 with the Gr numbers varying between 10^3 and 10^9 , Re numbers varying between 70 and 1000 and Bi numbers at the top surface of the shaft varying between 1 and 100. The temperature difference, ΔT , was maintained at 80°C .

3.1 Comparison with experimental data

Figure 2 illustrates the flow development represented by the vertical velocity profiles at four different heights of $y = 0.167 H$, $0.5 H$, $0.75 H$ and $0.95 H$ for $Bi = 1$, $Re = 75$ and $Gr = 6 \times 10^3$. The model predictions agreed very well with the measurements for all the respective heights along the shaft. Near the inlet, $y = 0.167 H$, the upwards movement of the hot air along the shaft was characterised by steep velocity gradients close to the shaft walls with the appearance of two velocity peaks. Near the outlet, $y = 0.95 H$, the vertical velocity being negative on the right hand side of the shaft wall signified the dilution of the hot air with the cold air entrained into the shaft from the top exhaust. On the opposite side, the hot air travelling upwards along the shaft was indicated by the positive vertical

velocity. In between these heights, the flow of the hot air along the shaft appeared to be in a transitional stage.

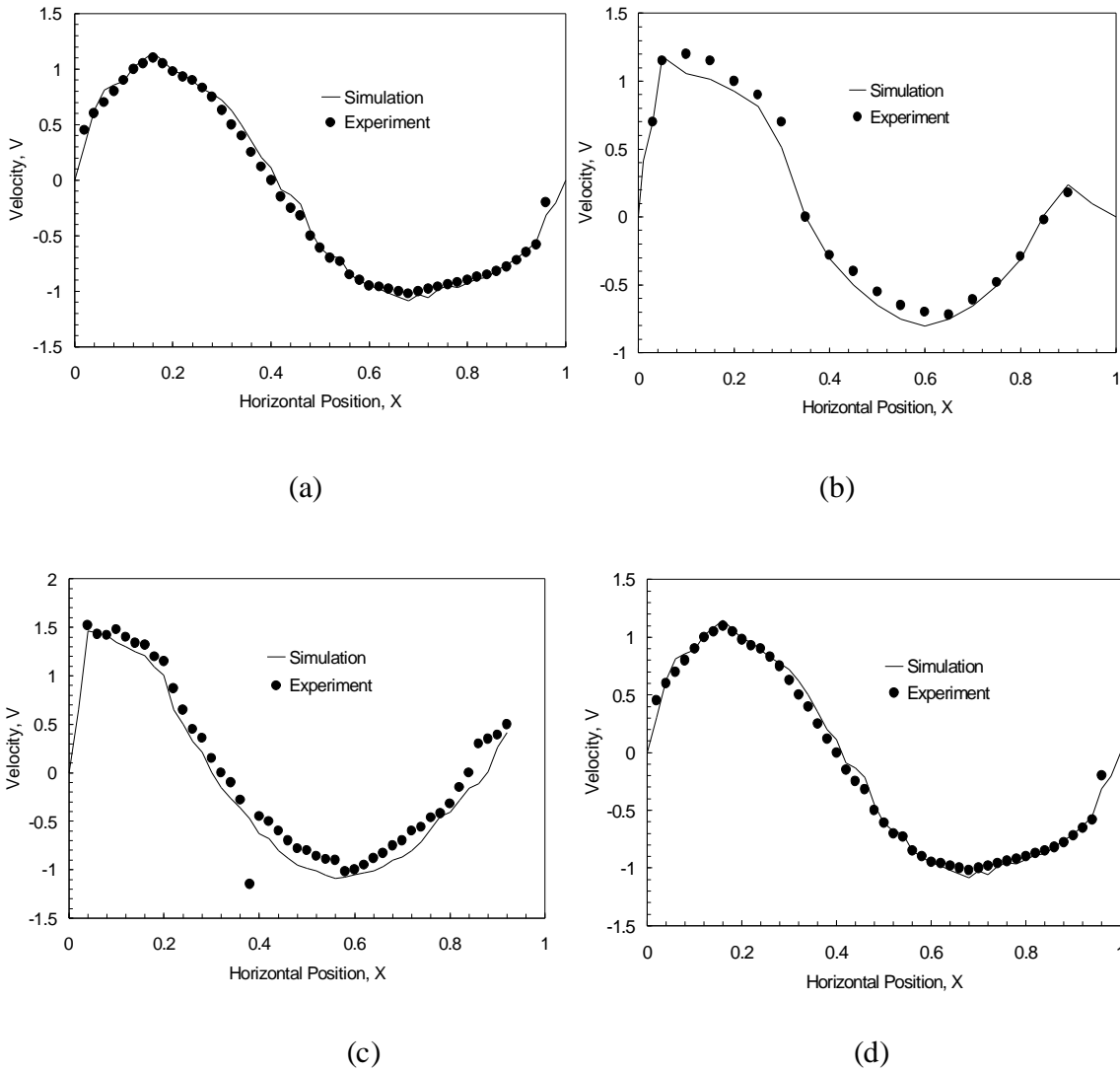


Figure 2 Comparison of simulation and experimental vertical velocity profiles across the shaft for $Re = 75$ and $Gr = 6 \times 10^3$ at different heights: (a) $y = 0.167 H$, (b) $y = 0.5 H$, (c) $y = 0.75 H$ and (d) $y = 0.95 H$.

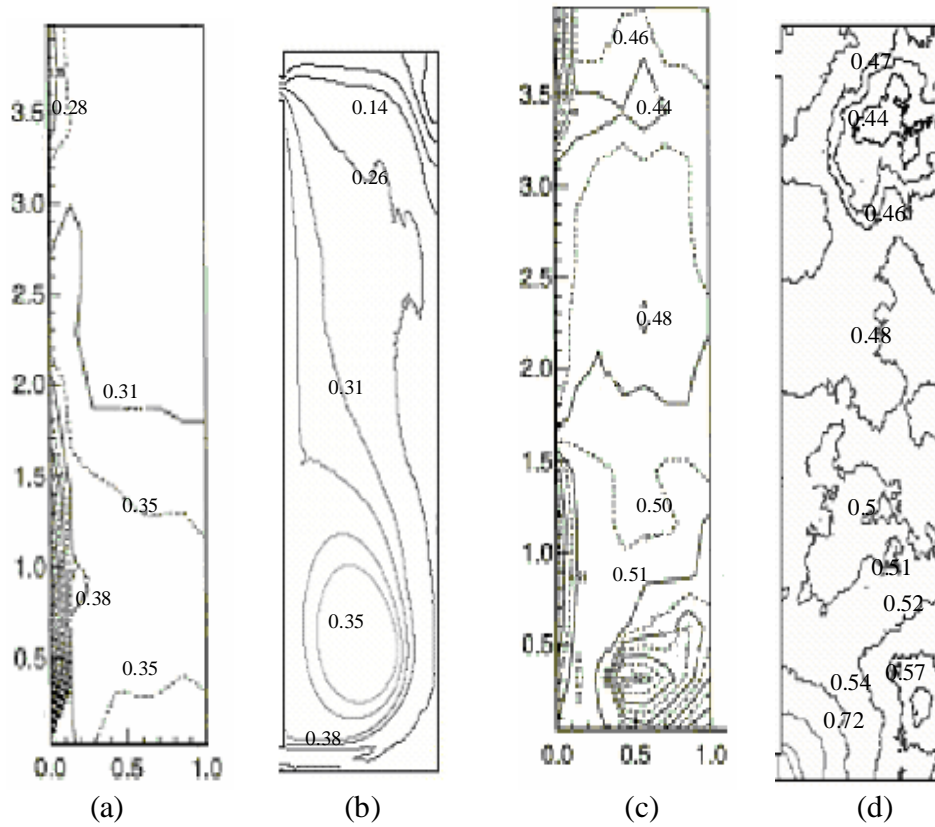


Figure 3 Isotherms of simulations and experiment in the vertical draft for different Re and Gr number: (a) experiment results for $Re = 70$ and $Gr = 6 \times 10^3$, (b) simulation results for $Re = 70$ and $Gr = 6 \times 10^3$, (c) experiment results for $Re = 400$ and $Gr = 6 \times 10^3$ and (d) simulation results for $Re = 400$ and $Gr = 6 \times 10^3$.

Figure 3 presents the comparison between the measured and predicted isotherms at a fixed $Gr = 6 \times 10^3$ for $Re = 70$ and 400 . These results demonstrate the competing modes dominating the fluid motion by either the forced or free convection or a combination of both. For the low Re case, the predicted isotherms were found to be significantly different from the measurements. One possible explanation for the discrepancy could be the adiabatic condition applied for the temperature at the wall surfaces. The buoyancy-driven flow mainly by free convection was allowed to penetrate deeper into the confined space of the shaft since there were no heat losses across the shaft walls. A convective boundary condition, imposed at the top surface of the shaft, could be similarly applied to these walls to halt the strong penetration of the buoyancy-driven flow due to some fraction of the heat escaping into the surroundings. This thereby could make the temperature distribution more comparable to the measurements. Nevertheless, the actual Bi numbers to be employed are not easily known. A sensitivity study of the effect of different Bi numbers was performed on the hot gas temperature at the exhaust outlet, which more details of the investigation are described below. On the contrary, for the higher Re case, the fluid motion driven more by force convection promoted more vigorous mixing of the

hot air with the cold air drawn from the top exhaust. There were still some discrepancies between the predictions and measurements especially near the wall regions but better agreement was achieved especially in the middle region of the shaft.

3.2 Parametric analysis

The vertical velocity and temperature profiles in Figure 4 were obtained by varying the Gr numbers of 10^3 , 10^6 and 10^8 whilst fixing the Re number to be 100. In Figure 5, however, the results were represented by varying the Re numbers of 100, 500 and 1000 for a fixed Gr number at 10^6 . This parametric investigation aimed to determine the extent of the free or forced convection modes affecting the buoyancy-driven flow behaviour of the hot gas. All the above profiles were plotted at the mid-height of the shaft, i.e. at $y = 0.5 H$. In general, the flow and heat characteristics were rather similar when the fluid motion was agitated by either increasing the Re or Gr numbers. For the bounding cases in Figures 4 and 5, the maximum values of the vertical velocity, whether positive (upward flow) on the left hand side of the shaft or negative (downward flow) on the opposite side, were only marginally higher for the case of high Re number in comparison to the case of high Gr number. The temperatures for the case of increasing Re numbers at a fixed Gr number were found to follow the similar trend illustrated by the vertical velocity profiles. At high Re number, the gas temperatures were found to be closed to the inlet temperature. However, the temperatures showed the reverse trend for the case of increasing Gr numbers at a fixed Re number where they were significantly lower at high Gr number because of the vigorous mixing promoted between the incoming hot air from the inlet and the cold air being entrained from the top exhaust. This indicated a complex flow structure represented by the presence of recirculation convective cells.

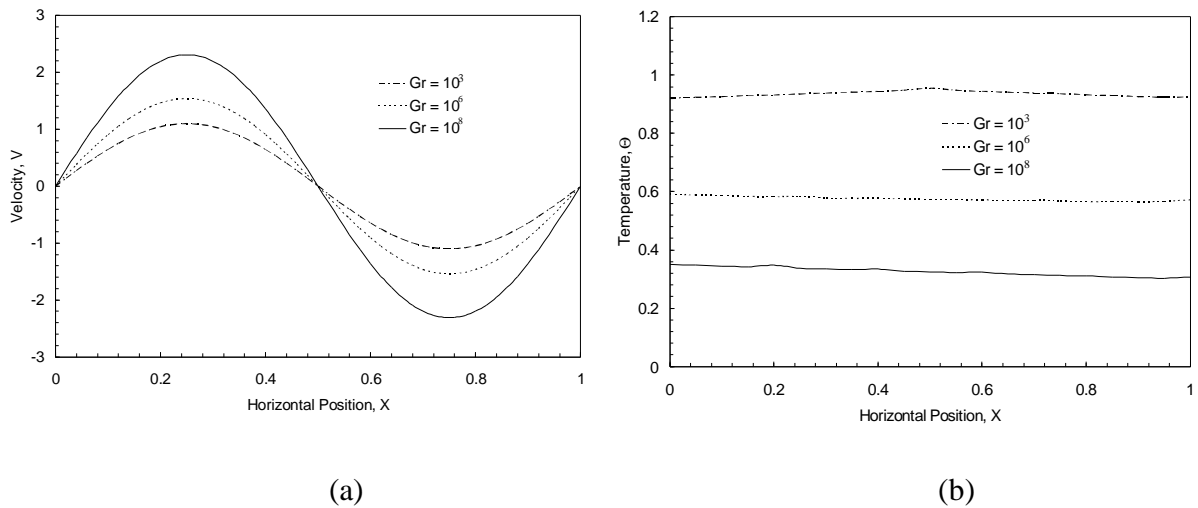


Figure 4 Simulation results for $Re = 100$ and $Gr = 10^3, 10^6$ and 10^8 across the shaft horizontal distance at $y = H/2$: (a) Vertical velocity and (b) Temperature

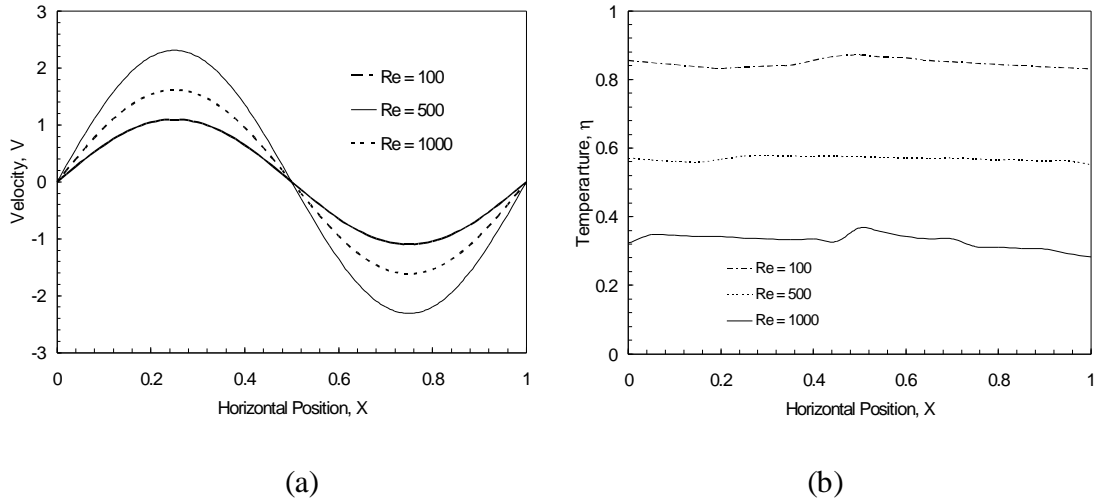


Figure 5 Simulation results for $Gr = 10^6$ and $Re = 100, 500$ and 1000 across the shaft at $y = H/2$: (a) Vertical velocity and (b) Temperature.

Thus far, the analysis has only concentrated on the fire-induced flow at laminar conditions because of the reduced-scaling of the model being solved. In a full-scale fire scenario, the Gr and Re numbers would easily lie in the turbulent regime because of the large scaling associated to an actual building structure in comparison to those of the reduced-scale model. Figures 6 and 7 illustrate the comparison of the flow behaviour by the predicted streamlines and isotherms at laminar and turbulent conditions. For laminar flow, where the Re and Gr numbers are low, the streamlines revealed a uniform flow near the inlet and top exhaust regions. However, as the hot air entered the shaft, the streamlines indicated a recirculating cell driven by the buoyancy forces in the core region of the shaft. The flow structure also revealed very thin boundary layer flows along the vertical adiabatic shaft walls. For turbulent flow, at high Re and Gr numbers, because of the vigorous mixing promoted by the energetic turbulent eddies, the fluid flow and heat transfer were found to be more evenly distributed throughout the core region of the shaft. The streamlines looked rather symmetry about the mid-height plane of the shaft. For the isotherms when the Gr number is small, the variations in the middle and outlet were small. However, multi-cells being present in the middle and outlet of the shaft at high Gr number revealed strong localized recirculation buoyant-induced turbulent flows that promoted cooling of the hot air from the inlet and heating of the cold air drawn from the top exhaust.

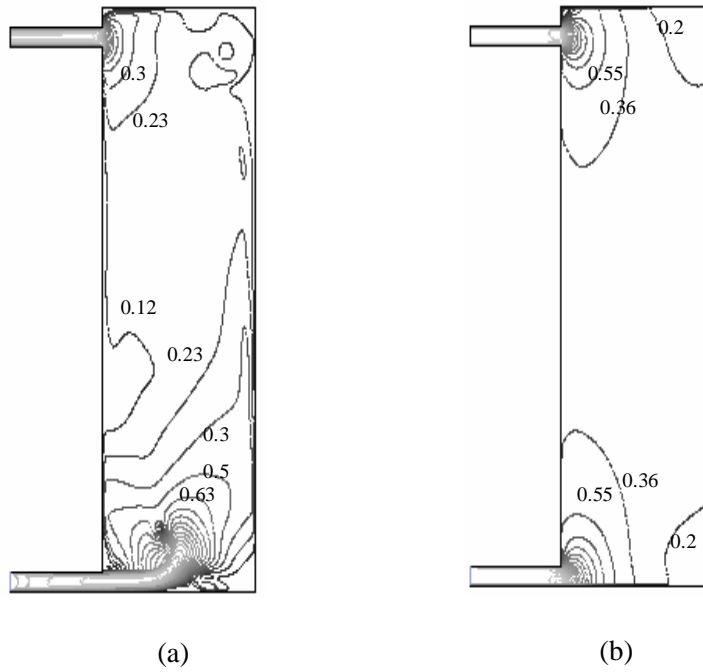


Figure 6 Simulated streamlines: (a) laminar condition – $Re = 70$ and $Gr = 10^3$ and (b) turbulent condition – $Re = 1000$ and $Gr = 10^9$.



Figure 7 Simulated isotherms: (a) laminar condition – $Re = 70$ and $Gr = 10^3$ and (b) turbulent condition – $Re = 1000$ and $Gr = 10^9$.

4. CONCLUSIONS

The fire-induced flow in a vertical shaft has been numerically simulated. The results were validated against the experimental data of Mercier and Jaluria [9]. Good agreement was achieved between the predictions and measurements. When the Gr number or Re number was low, a wall plume of hot gases could be seen developing in the interior region of the vertical shaft. However, when the Gr number or Re number was high, the flow structure was represented by a thin boundary layer along the wall with a large recirculating convective cell. The velocity field was found to be similar when the Gr number or Re number was varied but the temperature field behaved otherwise in particular the temperatures showed the reverse trend for the case of increasing Gr numbers at a fixed Re number.

REFERENCES

1. H. W. Emmons, The Prediction of Fire in Buildings, *9th Symposium (International) on Combustion*, Combustion Institute, pp. 1101-1110, 1987.
2. J. Cannon and E. Zukoski, Turbulent Mixing in Vertical Shafts Under Conditions Applicable to Fires in High Rise Buildings, Internal Report, California Institute of Technology, CA, 1976.
3. J. G. Quintiere, Perspective on Compartment Fire Growth, *Comb. Sci. Tech.*, vol. 39, pp. 11-54, 1984.
4. S. Y. Kim and Y. Jaluria, Basic Considerations in Combined Buoyancy-Induced and Forced Flow in a Vertical Open Shaft, *Num. Heat Transfer*, Vol. 34, pp. 519-536, 1998.
5. G. P. Mercier and Y. Jaluria, Fire-Induced Flow of Smoke and Hot Gases in Open Vertical Shafts, *Exp. Thermal Fluid Sci.*, vol. 13, pp. 77-84, 1999.
6. E. Launder and D. B. Spalding, The Numerical Computation of Turbulent Flows, *Comp. Meth. Appl. Mech. & Eng.*, vol. 3, pp 269-289, 1974.
7. FLUENT, version 6.0, *Computational Fluid Dynamics User's Guide manual*, Hanover, New Hampshire, 2001.
8. A. A. Mohamad, Natural Convection in Open Cavities and Slots, *Num. Heat Transfer*, vol. 27, pp. 705-716, 1995.